New Insights into the Metal Center of 3-Deoxy-D-*arabino*-heptulosonate 7-Phosphate Synthase†

Peter A. Jordan,‡ D. Scott Bohle,*,‡ Cecilia A. Ramilo,§ and Jeremy N. S. Evans§

Department of Chemistry, University of Wyoming, Laramie, Wyoming 82071-3838, and Department of Biochemistry and Biophysics, Washington State University, Pullman, Washington 99164-4660

Received February 5, 2001; Revised Manuscript Received April 16, 2001

ABSTRACT: Metal binding properties for a series of metal-substituted forms of 3-deoxy-D-*arabino*-heptulosonate 7-phosphate synthase, DAHPS(Tyr), have been followed by UV−vis and EPR spectroscopy. The results show that there are two metal species present at pH = 7.0 and these are coordinated in a distorted metal binding site with a mixed nitrogen and oxygen donor atom coordination set. There is no spectroscopic evidence for strong M−S interactions in this system at any pH. Metal saturation occurs at a substoichiometric ratio of 0.8−0.85 metal/monomer, and the binding trends mirror previously published enzyme activity profiles. There is a conformational change for CuDAHPS under basic conditions, and equivalent protein handling for apoDAHPS leads to apparent loss of metal binding ability. Addition of the substrate PEP does not alter the UV−vis spectra, but there are small changes in the EPR spectra of CuDAHPS(Tyr). Further addition of the substrate analogue A5P has no effect on either spectra. Taken together, these results serve to link previous studies on enzyme activity with the recently determined X-ray crystal structure for DAHPS(Phe) and represent the first detailed spectroscopic characterization of the metal binding properties of DAHPS(Tyr).

The enzyme 3-deoxy-D-*arabino*-heptulosonic acid 7-phosphate synthase (DAHPS)[1] catalyzes the first committed step in the shikimate pathway, which leads to the biosynthesis of aromatic amino acids in microorganisms and plants (*1*, *2*). DAHP synthases can be separated into two broad groups: those from plants and those from bacteria (*3*, *4*). The reaction catalyzed is the formation of DAHP and inorganic phosphate from phosphoenolpyruvate (PEP) and erythrose 4-phosphate (E4P) (eq 1).

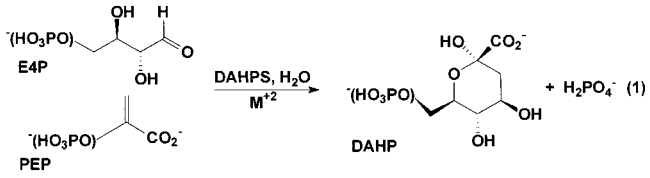

In *Escherichia coli* there are three isozymes, DAHPS(Phe), DAHPS(Tyr), and DAHPS(Trp), each subject to feedback regulation by one of the three aromatic amino acids (*5*). These isozymes are encoded by the genes *aroG*, *aroF*, and *aroH*, respectively, and the corresponding nucleotide sequences of these genes from *E. coli* have been determined, cloned, and overproduced (*6*−*11*). There is 41% sequence identity between the proteins predicted from the three gene products. For a catalytically competent system the enzyme is in an aggregated form and contains a single divalent metal ion per subunit. The enzymes DAHPS(Tyr) and DAHPS(Trp) associate as homodimeric units while DAHPS(Phe) forms a homotetramer. The role of the metal may be for catalysis and/or structural integrity. The identity of the metal ion in vivo remains elusive, and different metal ions (Cu^{2+}, Co^{2+}, Fe^{2+}) have been found in the protein expressed from the same gene either under identical or similar conditions (*6*, *10*−*17*). In pure preparations of DAHPS(Tyr), the native metal was found to be either a Cu, Zn, or Fe, all in substoichiometric amounts (*11*). In vitro, the enzyme can be activated by a variety of divalent cations of Cd, Mn, Zn, Fe, Mg, Co, and Cu (*6*, *10*, *11*). The diverse nature of these metal activators suggests that their role is either structural or as a Lewis acid but is not based upon any redox cycle. No other cofactors have been identified for DAHPS from bacteria, although the major enzyme from plants, MnDS, is known to require reductants such as DTT (*18*, *19*).

Previously, it has been proposed by Bauerle and coworkers (*10*) that the metal probably polarizes the carbonyl carbon of E4P and facilitates nucleophilic addition at that carbon by C-3 of PEP. However, more recent work from the same laboratory on the X-ray crystal structures of the M·DAHPS(Phe), M = Pb^{2+} (catalytically inactive as a PEP complex) (*20*) and Mn^{2+} (catalytically active as a PGL complex) (*21*), has demonstrated that the former structure

† This work was supported, in part, by a grant from the NIH (R01 GM43215 to J.N.S.E.) and from the Burroughs-Wellcome Fund for a New Initiatives in Malaria Research Award (1001564) to D.S.B.

* Corresponding author. Tel: 1-307-766-2795. Fax: 1-307-766-2807. E-mail: Bohle@uwyo.edu.

‡ University of Wyoming.

§ Washington State University.

[1] Abbreviations: A5P, arabinose 5-phosphate; DAHP, 3-deoxy-D-*arabino*-heptulosonate 7-phosphate; DAHPS, 3-deoxy-D-*arabino*-heptulosonate 7-phosphate synthase, with respect to the feedback-sensitive isozyme DAHPS(x), where x is the amino acid Tyr, Phe, or Trp [all residues are numbered according to the crystal structure of DAHPS(Phe)]; DS, plastid localized plant DAHPS; DTT, dithiothreitol; E4P, erythrose 4-phosphate; EPR, electron paramagnetic spectroscopy; PEP, phosphoenolpyruvate; PGL, 2-phosphoglycolate; Tf, transferrin.

10.1021/bi010238f CCC: $20.00
Published on Web 06/22/2001

has a weak π-complex with the olefin−carboxylate moiety of PEP (*20*) while the latter has a carboxylate−Mn^{2+} bond to the PGL (*21*). The metal is clearly intimately required at the active site, and these structures are a major advance in our understanding of the catalytic mechanism and the method of allosteric control by the appropriate aromatic amino acids. Both structures are homotetramers comprised of two tight dimer units and where the geometry of each monomer is based upon a $(\beta/\alpha)_8$ barrel with some additional elements. The active site is in a cleft at the C-terminal end of the barrel. The metal binding site lies at the bottom of this cleft and is covered by the PEP. It is postulated that E4P then occupies the remaining space in the cleft and is partially exposed to solvent. This geometry would enforce the required stereochemistry of the pseudo-aldol condensation in eq 1. In both structures the same amino acids, Cys61, His268, Glu302, and Asp326, interact to varying extents with the metal. All of the charged residues within 8 Å of the metal site are invariant among microbial DAHPS enzymes. The putative site for aromatic amino acid binding is remote from the active site (>14 Å).

Solution-state studies have also probed enzyme structure and function through the use of steady-state kinetics and random mutagenesis (*22*). A number of critical residues have been identified with these techniques (*8*, *17*, *23*−*25*). Notable among these is the observation that Cys61 is essential for catalytic activity (*23*). Furthermore, enzymatic activity can be linked to the oxidation state of the enzyme, and disulfide bond formation between Cys61 and Cys328 compromises function (*26*). Enzymatic activity profiles for each isozyme describe bell-shaped curves with respect to pH, with a maximum at approximately pH = 7.0 (*11*). This is in contrast to DAHPS from plants, where the two known isozymes exhibit very different activity profiles, with MnDS active at pH = 7.0 and CoDS active at pH = 10.0 (*27*). Spectroscopic studies on these enzymes have been limited to single UV−vis spectra for the Cu^{2+}, Co^{2+}, and $Fe^{2+/3+}$ derivatives (*6*).

We have previously designed a highly efficient system for the overexpression and purification of DAHPS(Tyr) from *E. coli* (*11*) and have also shown that DAHPS(Tyr) requires a divalent metal cation in that removal of the metal by EDTA results in the loss of enzymatic activity (>96%), but full activity can be restored upon reconstitution of the apoenzyme with a variety of divalent metal cations. In this work, to characterize the structural features of the binding site of this enzyme, the native metal in the enzyme was replaced with several divalent metals, most notably, Cu^{2+}, a complex with an EPR-active center shown to retain at least 44% of wild-type activity (*11*). Here, we report extensive characterization of the metal binding properties of DAHPS(Tyr) and examine the effects of pH and substrate on the metal center, using a combination of UV−vis and EPR spectroscopy.

MATERIALS AND METHODS

Purification of DAHP Synthase (Tyr). The enzyme was purified from *E. coli* according to the method previously reported (*11*). All manipulations were carried out at 4 °C.

Enzyme Activity Assay and Protein Determination. DAHPS(Tyr) activity was determined by measuring the rate of disappearance of PEP (*16*). Protein concentrations were determined by the method of Bradford (*28*) relative to bovine serum albumin, which are known to correlate reasonably well with spectrophotometric methods based on a calculated extinction coefficient for A_{280} of 24 540 M^{-1} cm^{-1} for the fully reduced enzyme.

Preparation and Reconstitution of Apoenzyme. DAHPS (~2 mg/mL) in 50 mM potassium phosphate buffer (pH = 6.8, 15% ethylene glycol) was dialyzed against 10 mM EDTA until the activity was less than 3% of the initial value (~24 h). The metal−EDTA complex and excess EDTA were removed by dialysis (three exchanges every 4 h) against transition metal-free buffer. The apoenzyme was assayed for enzymatic activity. Throughout these preparations careful control of pH was maintained to avoid denaturation.

UV−Vis Spectroscopy. Data were collected on a Hewlett-Packard HP 8453 diode array spectrometer. Sample volumes were 400 μL or 1.5 mL. All solutions were mixed thoroughly following addition and stirred continuously thereafter.

Metal Binding. Metal solutions used were freshly prepared 2 mM $Cu(NO_3)_2$ or 1 mM $CuSO_4$, fresh 2 mM $CoAc_2$, 2 mM $MnCl_2$, and 1 mM $Fe(NO_3)_3$. A period of 5 min was allowed between metal additions.

pH Titration. A mixed buffer system, 10 mM Mes, 10 mM Hepes, 10 mM Tris, 50 mM KCl, and 10% glycerol, with additions of 1 mM HCl or NaOH was used throughout. The pH of the sample was checked before and after each spectrum was recorded using a thin-stemmed combination electrode.

EPR Spectroscopy. A Bruker EMX system operating at 9.66 GHz for X-band was used for data acquisition. This was equipped with a dual mode cavity coupled to an Oxford Instruments liquid helium flow cryostat for low-temperature work. Samples for EPR spectroscopy were prepared by treating metal-free apoDAHPS with 1 equiv of metal ion for ca. 20 min, followed by two repeats of an ultrafiltration and buffer wash step. The resulting solution was transferred to an EPR tube, quench frozen in liquid nitrogen, and maintained at 77 K until used for measurement.

RESULTS

Metal Binding to DAHPS(Tyr). (A) CuDAHPS. Addition of Cu^{2+} to metal-free apoDAHPS(Tyr) results in a new peak at 355 nm in the UV−vis spectrum (Figure 1a). This is consistent with a ligand to metal charge-transfer band based upon a nitrogen or sulfur donor atom ligand (*29*). In accord with prior results (*6*), there is no absorption in the 600 nm region, indicating that the sulfur from Cys61 is not a ligand at pH = 7.0. The metal binding profile for replicate titrations of apoDAHPS with Cu^{2+} is shown in Figure 1b. The saturating metal/enzyme ratio is 0.8−0.85 for this set of titrations, a value identical to that found for the uptake of Mn^{2+} by DAHPS(Phe) (*10*). We note that the metal analysis of previous samples revealed only fractional metal occupancy (<10%) of the purified, metal-reconstituted, protein (*11*). Recent work has demonstrated that the isozyme DAHPS(Phe) is sensitive to oxidation, which leads to inactivation (*26*). However, the convergence of these three completely separate measurements suggests that these fractional uptake values are not entirely adventitious. Kinetic traces for the addition of $CuSO_4$ to DAHPS(Tyr) show the metal binds rapidly to the apoenzyme ($t_{1/2}$ ~ 20 s) (Figure 1c,d). Analysis of the kinetic traces at different wavelengths, and for the

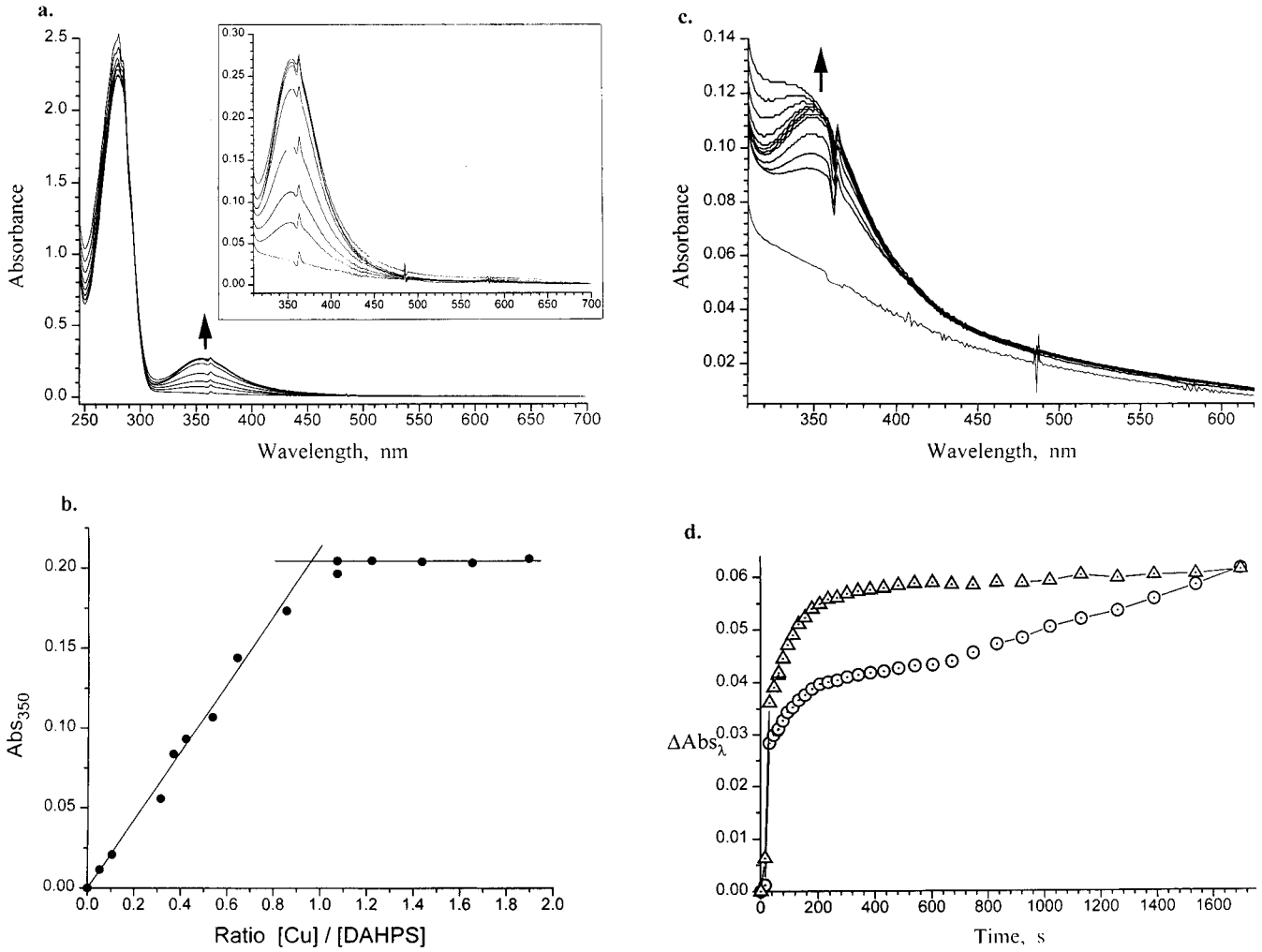

FIGURE 1: UV−vis spectra for the addition of Cu^{2+} to DAHPS(Tyr). (a) Overlay spectra for the addition of 2 mM $Cu(NO_3)_2$ to 68 μM DAHPS(Tyr). [Cu^{2+}], μM: i, 0; ii, 10; iii, 20; iv, 30; v, 39; vi, 49; vii, 58; viii, 77. (b) Binding profile at A_{350} for the addition titration shown in Figure 1a. (c) Overlay spectra with time following the bulk addition of 20 μM $CuSO_4$ to 42 μM DAHPS(Tyr): Time, s: i, 31; ii, 63; iii, 110; iv, 180; v, 270; vi, 384; vii, 540; viii, 750; ix, 1020; x, 1390; xi, 1700. (d) Kinetic traces at 330 nm (○) and 350 nm (△) extracted from Figure 1c.

entire UV−vis spectrum, indicates that under these conditions, once formed, the CuDAHPS complex undergoes a slow conformational change. This is clearly seen in the biphasic nature of the change in absorbance at 330 nm with time. The time course for this conformational change is much slower than for the initial binding reaction. In this experiment, the enzyme was present in excess, and the change in absorbance observed at 350 nm indicates ~100% coordination of the Cu^{2+}. This suggests that the subsequent conformational change is specific and not based upon enzyme oxidation due to free Cu^{2+} in solution.

The X-band EPR spectrum of CuDAHPS at pH = 7.0 shows two axial signals (Figures 2a and 4a). The *g*-values for these two signals are $g_{||} = 2.24$ and $g_{\perp} = 2.036$ and $g_{||} = 2.28$ and $g_{\perp} = 2.019$ (Table 1). It was not possible to distinguish any variable temperature or power dependence in these signals, so correlation of $g_{\perp}$ and $g_{||}$ is based upon the behavior of the system with varying pH (see later). Multifrequency EPR spectroscopy of this system is required to more rigorously verify these assignments (*30*−*33*).

The high-field signal observed above 3450 G is an "angular anomaly". Angular anomalies, also called overshoot lines, are a feature of Cu(II) EPR signals observed at X-band frequency when $A_{||}$ is large and $g_{||}$ is small. They are based upon the angular dependence of the hyperfine splitting, which drives the ^{Cu}A ($m_I = -3/2$) line to higher field than the $g_{\perp}$ manifold. Further treatment of this problem is available in a number of texts (*31*, *34*−*36*). As shown in Figure 3, hyperfine coupling is observed in the $g_{\perp}$ region, and it is unambiguously highlighted in the second derivative of the EPR spectrum in Figure 3b. The observed splitting, which results in at least six lines, can result from a combination of $^{Cu}A_{\perp}$ and $^{N}A_{\perp}$ hyperfine interactions and is further complicated by overlap by the two spectra in this region. Variable power and temperature studies showed that the Cu EPR signal begins to saturate above 1 mW at 20 K and is significantly reduced in intensity above 40 K.

(B) CoDAHPS. As reported previously (*6*), the UV−vis spectrum for Co(II)DAHPS(Tyr) shows a weak absorption at 500 nm, in addition to several weak bands due to a minor CuDAHPS impurity. It was not possible to completely remove the contaminating Cu^{2+} even in the presence of excess Co^{2+}. This may be due to DAHPS(Tyr) having a higher affinity for Cu^{2+} than Co^{2+} or slow kinetics for metal exchange. Using the DAHPS(Phe) isozyme, Stephens and Bauerle (*10*) reported relative metal affinities to be Co^{2+} >

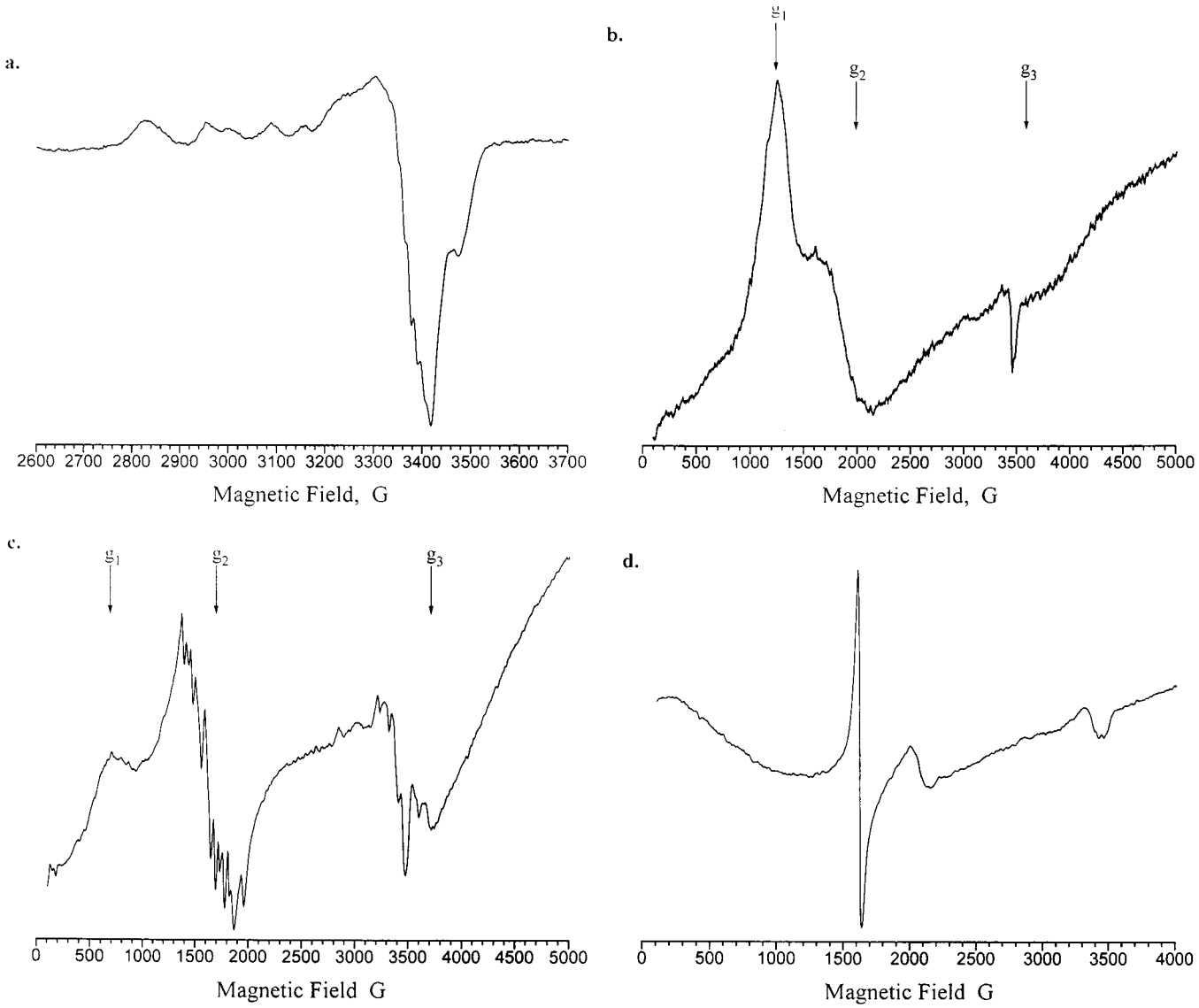

FIGURE 2: Low-temperature X-band EPR spectra for metal-substituted DAHPS(Tyr). (a) Cu(II)DAHPS at pH = 7.0. Conditions: 20 K, 0.2 mW power, and 5 G modulation amplitude. (b) Co(II)DAHPS at pH = 7.0. Conditions: 6.5 K, 0.2 mW power, and 10 G modulation amplitude. (c) Mn(II)DAHPS at pH = 7.0. Conditions: 10.0 K, 2 mW power, and 10 G modulation amplitude. (d) Fe(III)DAHPS at pH = 7.0. Conditions: 9.0 K, 2 mW power, and 10 G modulation amplitude.

Table 1: Spectroscopic (EPR) Parameters for Metal-Substituted DAHPS(Tyr)

metal	pH	g_1	g_2	g_3	A, G
Co(II)	7.0	5.6	3.8	1.90	
Mn(II)	7.0	9.7	4.32	1.92	90
	7.0	9.7	4.18	1.92	90

metal	pH	$g_\perp$	$g_\parallel$	$A_\parallel$, G	$A_\perp$, G
Cu(II)	7.0	2.036	2.244	150	14
	7.0	2.019	2.285	130	
	7.5	2.036	2.214	187	15
	7.5	2.019	2.28	~125	
	8.7	2.036	2.206	190	16.5
+1 mM PEP	8.7	2.038	2.217	187	15

Cu^{2+}. However, this work was based upon competitive enzyme kinetics and did not measure metal coordination directly. Later work, again by Bauerle (*26*), has demonstrated the oxidative inactivation of the enzyme in the presence of large quantities of Cu^{2+} or Fe^{3+}, so this may explain the relative affinities observed.

The EPR spectrum of CoDAHPS shows a single, broad, rhombic signal (Figure 2b). This is consistent with transitions from a single Kramers doublet of a high-spin, $S = {}^3/_2$, system (*37*). The *g*-values are 5.6, 3.8, and 1.90 and suggest either a distorted tetrahedral or tetragonal coordination (*37*, *38*). Of these two possibilities, the weak UV−vis bands (described above but data not shown) are most consistent with the latter, and we note that no hyperfine coupling to the Co^{2+} nucleus ($I = {}^7/_2$) is observed for any of the resonances. In common with other Co−protein complexes, the EPR signal is very sensitive to temperature and microwave power. The signal is completely lost above 15 K and shows signs of saturation at 6.5 K above 1 mW power.

(C) MnDAHPS. For the titration of DAHPS with Mn^{2+} no new absorption peaks are observed in the UV−vis spectrum. Of all the metal-substituted forms of DAHPS(Tyr), the Mn-substituted form was the least stable, and routine sample manipulation frequently leads to facile demetalation. Under the experimental conditions employed, Mn^{2+} would not be expected to cause oxidative degradation of the

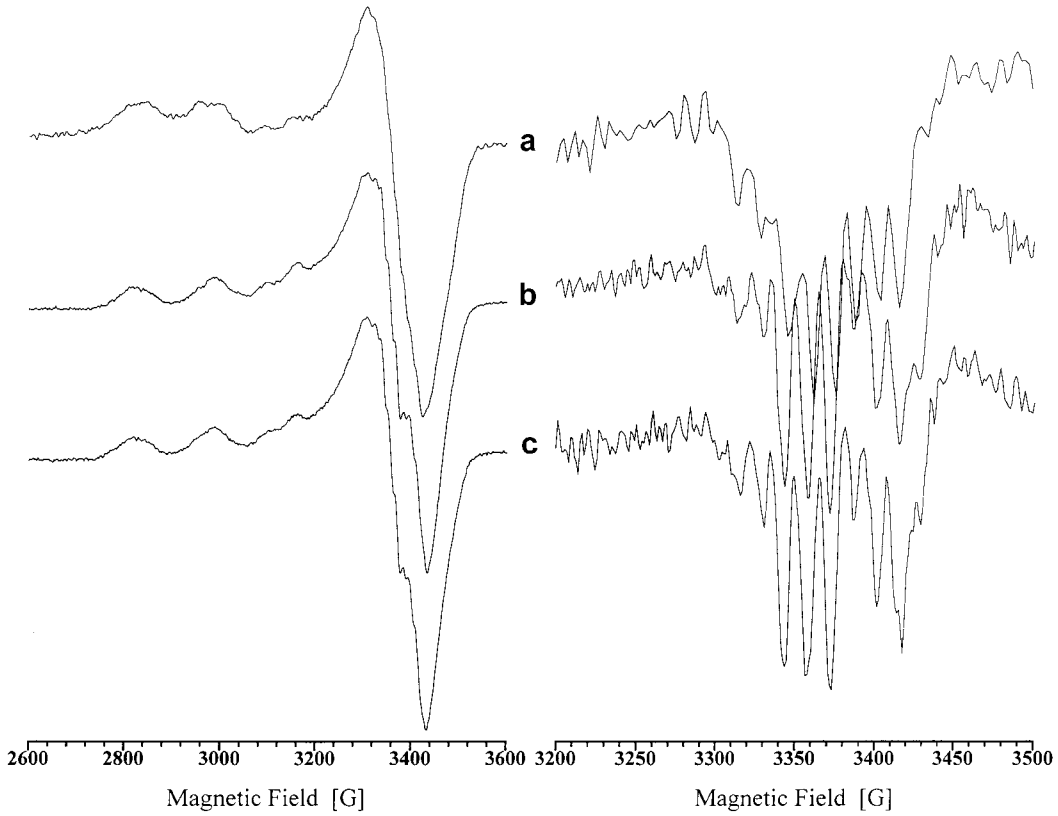

FIGURE 3: Low-temperature X-band EPR spectrum for the addition of PEP and A5P to Cu(II)DAHPS(Tyr): (a) CuDAHPS; (b) CuDAHPS + 1 mM PEP; (c) CuDAHPS + 1 mM PEP + 1 mM A5P. In all three plots the measured data are shown on the left and the second derivative on the right. Conditions for each measurement: pH = 7.0, 21−23 K, 1 mW, and 6 G modulation amplitude.

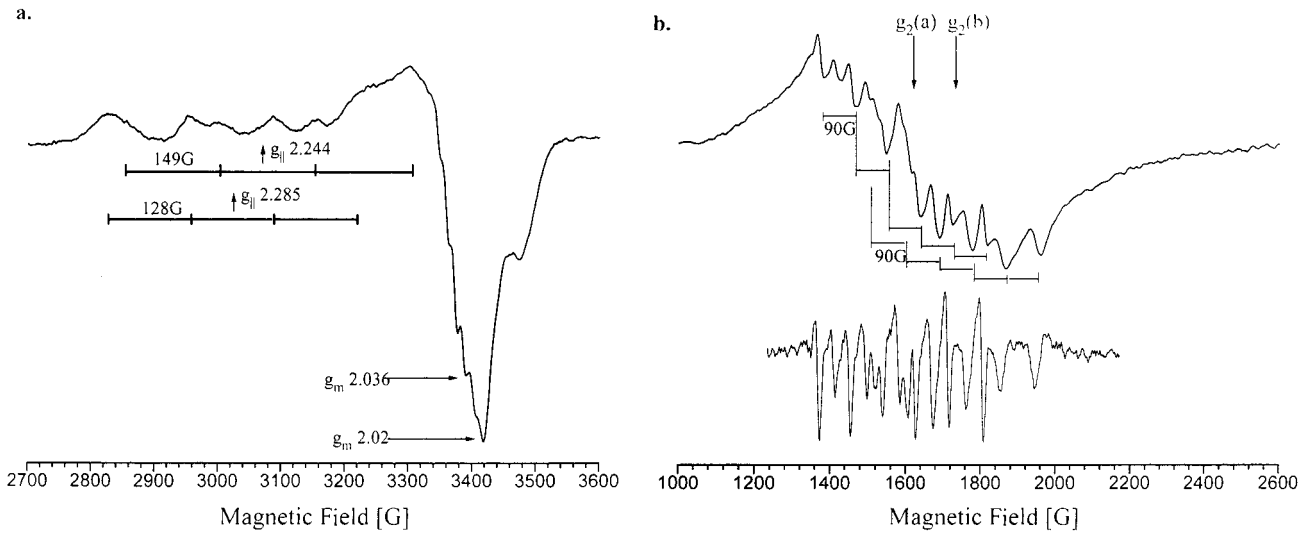

FIGURE 4: Assignment of EPR spectra. (a) Cu(II)DAHPS at pH = 7.0. Conditions: 20 K, 0.2 mW power, and 5 G modulation amplitude. (b) Mn(II)DAHPS at pH = 7.0. Conditions: 10.0 K, 2 mW power, and 10 G modulation amplitude. The lower trace is the second derivative of the EPR spectrum, shown on the same *X*-axis scale.

enzyme, and it is significant that MnDAHPS(Tyr) has the highest specific enzymatic activity of any metal substituents including wild type (*11*). Stephens and Bauerle (*10*) reported that only 80% saturation of DAHPS(Phe) was achieved following exposure to a 10-fold excess of metal. It is possible that trace amounts of Fe^{3+} impurities could be responsible for oxidative damage. Indeed, when manganous chloride is used as a starting salt, significant quantities of Fe(III)DAHPS are observed in the EPR spectrum. This is analogous to the Co/Cu system discussed earlier and, again, could be due to relative binding affinities or the kinetics of metal exchange. Use of manganous acetate almost eliminates the FeDAHPS EPR signal. These samples are nevertheless still prone to metal loss during sample manipulation.

The EPR spectrum for MnDAHPS shows a broad rhombic signal for a high-spin system with *g*-values of 9.7, 4.3, and 1.92 (Figure 2c). The most striking feature of the spectrum is the resolved hyperfine splitting of the signal $g_2 = 4.3$, seen more clearly in Figures 2c and 4b. From this splitting, it is possible to resolve two sets of overlapping six-line patterns. This demonstrates that there are two different MnDAHPS complexes present at pH = 7.0, as previously

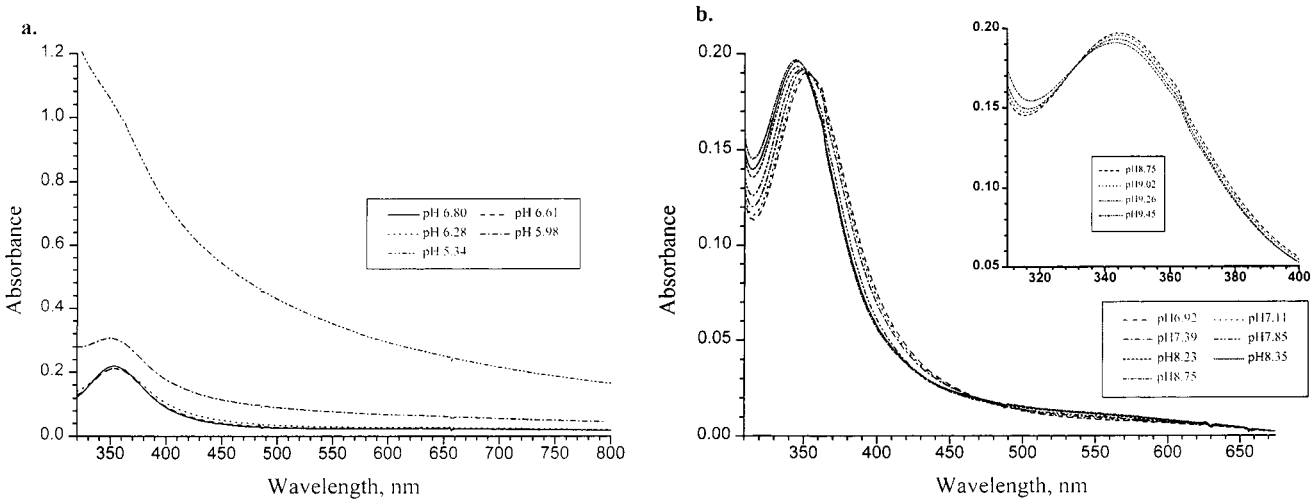

FIGURE 5: UV−vis spectra for CuDAHPS at different values of pH in a mixed 10 mM Mes, 10 mM Hepes, 10 mM Tris, and 50 mM KCl buffer system with 10% glycerol: (a) acidic pH adjusted with 1 mM HCl and (b) (and inset) basic pH adjusted with 1 mM NaOH.

observed for CuDAHPS. Although coordination geometry can sometimes lead to further splitting of the Mn hyperfine signals (*39*), the number and relative intensity of the signals observed here are consistent with two separate species. For manganese EPR, hyperfine splitting is often resolved for the $g \sim 2$ signal (e.g., MnTf, $MnAc_2$), and in this case, hyperfine splitting at $g = 4.3$ and not $g = 2.0$ serves as a useful marker for specific binding following titration with $MnAc_2$.

(D) FeDAHPS. The EPR spectrum of Fe(III)DAHPS at 9 K is dominated by an isotropic signal at $g = 4.3$, indicative of a high-spin $S = {}^5/_2$ sample in a rhombic field, as is found in many ferric siderophores (*37*, *47*). In the EPR spectrum of Fe(III)DAHPS this transition is relatively weak and has an intensity comparable to that of the bands from contaminating CuDAHPS and free iron which are observed at higher field. One possible origin for this diminished intensity could be dipolar interactions of vicinal high-spin iron in adjacent DAHPS subunits. No new signals are observed on elevating the temperature to 15 K.

pH Titrations of Apo- and CuDAHPS. (A) Acidic pH Range. The pH titration of CuDAHPS(Tyr) under acidic conditions (Figure 5a) demonstrates that this complex is stable in the range pH = 7.0 to pH = 6.0. Further decrease in pH to below pH = 6.0 compromises stability and results in significant protein precipitation. The metal stability profile, as judged from the CuDAHPS absorption band, mirrors the enzyme activity profile and demonstrates that the metal is required for activity. The acidic pH titration of apoDAHPS-(Tyr) has the same stability profile as does the metalated enzyme. This suggests that precipitation is due to inherent instability of the enzyme and is not triggered by metal release. Following removal of precipitated protein and restoration to pH = 7.4, the soluble apoenzyme was still able to bind copper.

(B) Basic pH Range. A number of interesting features are revealed in the titration of DAHPS(Tyr) with base (Figure 5b). The most significant feature for the copper-coordinated enzyme is a reversible conformational change that occurs between pH = 7.0 and pH = 8.5. This shows fairly well defined isobestic behavior with the new species having an absorbance maximum at 345 nm. This transition is accompanied by an increase in absorbance at 550 nm, possibly due to the introduction of a sulfur ligand, presumably from Cys61, into the copper coordination sphere. However, this is not entirely consistent with the increase in energy (shift to lower wavelength) observed for the ligand to metal charge-transfer band around 350 nm. This suggests a weaker metal−ligand interaction, with alternative explanations being that a possible conformational change results in a more distorted or less symmetrical coordination geometry or there is a decrease in charge of the copper complex. In this case the absorbance at 550 nm may be due to an increase in intensity of the Cu d−d transitions, which are formally forbidden (*29*). The relatively large changes observed in the EPR spectrum at high pH could be based upon any of these factors but is best supported by a change in coordination or charge. Up until pH = 8.75 the pH-dependent spectroscopic changes are reversible and suggest that there is an equilibrium transition in this pH range. Between $6 < \text{pH} < 7$ there are no significant changes in the EPR spectrum (data not shown). Further increases in pH from pH = 8.75 to pH = 9.45 (inset Figure 5b) led to a decrease in intensity for the UV−vis spectrum of CuDAHPS, which was presumably due to loss of the metal. Back-titration of this sample from pH = 9.5 to pH = 7.0 did not reverse the conformational change observed and only led to a further decrease in intensity of these bands. This suggests that a chemical modification is involved as opposed to a simple conformational change or deprotonation. As for the titration of CuDAHPS under acidic conditions, the UV−vis profile recorded mirrors the activity profile published previously (*11*). Indeed, the activity profile suggests a possible conformational change. Combining these two results shows that the new conformation retains enzyme activity, albeit slightly diminished.

The effect of pH upon CuDAHPS was also monitored using EPR spectroscopy, and these spectra are shown in Figure 6. In support of the UV−vis results, they demonstrate that there is a change in conformation between pH = 7.0 and pH = 8.7. The EPR spectrum at pH = 8.7 indicates that there is only one Cu species present, which is characterized by an axial pattern with $g_\perp = 2.03$ and $g_\parallel = 2.206$. The notable features of the spectrum are an intense line at high field, which is due to an angular anomaly, and the hyperfine splitting of the perpendicular signal. The key features of this

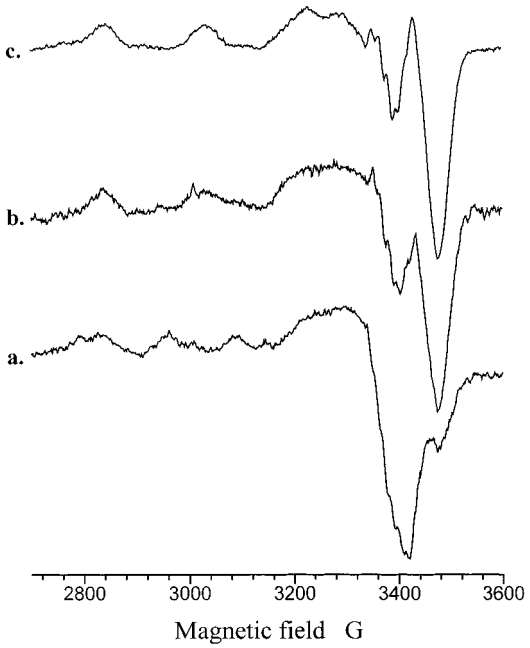

FIGURE 6: Low-temperature X-band EPR spectrum for the basic pH titration of Cu(II)DAHPS(Tyr). Conditions: (a) pH = 6.98, 20 K, 1.0 mW power, and 10 G modulation amplitude; (b) pH = 7.50, 20 K, 1.0 mW power, and 10 G modulation amplitude; (c) pH = 8.68, 20 K, 1.0 mW power, and 10 G modulation amplitude.

spectrum are common to CuTf, in which the Cu is coordinated to one nitrogen ligand and multiple oxygen ligands (*30*, *40*). At the intermediate pH = 7.5, two Cu species are present in different concentrations. The *g*-values for these species are $g_\perp = 2.019$ and $g_\parallel = 2.2$ for the minor component and $g_\perp = 2.036$ and $g_\parallel = 2.214$ for the major component. The former species was one of those present at pH = 7.0, while the latter appears closely related to the final species observed at pH = 8.7. Comparing the EPR spectra at pH = 7.5 and pH = 8.7 shows small differences in $g_\parallel$, $A_\parallel$, and particularly $A_\perp$. None of these spectroscopic features suggest cysteinyl sulfur coordination to the metal at any pH.

In contrast to the behavior of DAHPS in acidic conditions, under basic conditions the metal binding capacity of apoDAHPS is apparently lost following cycling to pH = 10. The protein appears to be more stable in basic conditions with only a minimal change in the UV−vis spectrum observed, due to precipitation, up to pH = 10. Back-titration to pH = 7.0 followed by addition of Cu^{2+} does not lead to the characteristic absorbance peak at 350 nm for CuDAHPS at this pH. There is a broad increase in the 350 nm region and an increase in the absorbance at 280 nm. This could be due to nonspecific copper binding or specific binding to an altered conformational state. Although the spectrum observed is similar to that seen following the bulk addition of Cu^{2+} to the enzyme in the absence of further data, it is not possible to distinguish between these two possibilities. To summarize, within the range $6 < pH < 8.7$ there are reversible spectroscopic changes by UV−vis and EPR spectroscopy, but at more extreme pH irreversible demetalation/denaturation occurs.

Addition of Substrate. There was no change in the UV−vis spectrum for CuDAHPS(Tyr) following the addition of the substrate PEP. In the EPR spectrum (Figure 3b) minor changes were observed with an increase in the resolution of the signals. This appeared to be due to a change in the relative populations of the two copper species observed at pH = 7.0. These results show that PEP is not a direct ligand to the metal but has some influence upon the overall first shell coordination sphere. This is in accord with the X-ray crystal structures for PbDAHPS(Phe) (*20*), in which the shortest distance between the Pb^{2+} center and the carbonyl oxygen of PEP is 3.74 Å. Similar observations can be made for the addition of PEP to CuDAHPS(Tyr) at pH = 8.7. At first glance, there appears to be a sharpening of the resonances, but a closer inspection reveals that there are small changes in both the *g*-values and the magnitude of the hyperfine coupling. Analysis of the second derivative spectrum in the $g_\perp$ region in the presence and absence of PEP shows that there is a divergence in the hyperfine splitting between the two sets of spectra. That is, the splitting increases with distance from $g_\perp$. This increase is larger in the absence of PEP, and eventually the peaks between the two spectra become out of phase and thus distinguishable. In fact, the hyperfine coupling pattern at pH = 7.0 overlays the pattern at pH = 8.7 in the presence of PEP, although the *g*-values do not. The basis of this divergence has not been determined. It may be due to a combination of nuclear ($^{Cu}A_\perp$) and ligand ($^{N}A_\perp$) hyperfine interactions. Coupling constants to different nuclear spin states are not necessarily equivalent. Again, this indicates that binding of the substrate PEP does not cause a major perturbation to the Cu coordination sphere. The small changes that are observed at pH = 8.7 suggest that the substrate binds to the enzyme at its normal position in this different conformation. This is expected as the enzyme retains activity at this pH.

No change was observed in the EPR spectrum for the addition of the substrate analogue A5P to a sample containing CuDAHPS and PEP (Figure 3c). This indicates that this substrate binds at a site less associated with the metal. It is known that DAHPS(Phe) can utilize A5P in place of E4P, although at a lower level of enzyme activity (*41*, *42*).

DISCUSSION

A combination of UV−vis and EPR spectroscopy was used to probe the metal binding properties of DAHPS(Tyr) and examine the role of the metal in enzyme activity. Previous studies have been limited to UV−vis spectroscopy and afforded little insight into the specific metal binding site. The low-temperature EPR results presented here are consistent with mixed ligation at pH = 7 including at least one His residue. Copper binding is stable under acidic conditions, to pH = 6.0, but the metal is readily lost below this as a result of protein precipitation. Stability is much greater under basic conditions and is marked by a conformational change at pH ~8.5. This is consistent with either a change in coordination, either ligand type or number, or a decrease in charge of the coordinated copper complex, or to alteration (shortening) of the Cu−S separation. Addition of the substrate PEP causes a slight change at the metal binding site, as evidenced by the EPR spectrum of CuDAHPS, but it is not enough to cause perturbation of the spin state in parallel experiments for CoDAHPS (data not shown). This is consistent with the substrate PEP influencing the coordination sphere but not being directly bound to the metal center. There was no further change in the EPR spectrum of

CuDAHPS upon addition of A5P, an analogue to the second substrate E4P (*41*, *42*).

The addition of small aliquots of Cu^{2+} to apoDAHPS-(Tyr) at pH = 7.0 was characterized by an increase in absorbance at 350 nm in the UV−vis spectrum. This absorbance was stable with time (>48 h at 4 °C) and gave indication of only one Cu^{2+} species. In contrast, the bulk addition of Cu^{2+} to apoDAHPS was characterized by two independent processes. The first step was indicative of specific metal binding to the enzyme. The basis of the second step is unknown. Under the reaction conditions, the enzyme was present in excess, and after the initial fast process, no unbound Cu^{2+} was present to promote random enzyme oxidation. It is possible that this second step is due to a kinetic rather than a thermodynamic phenomenon, with metal exchange occurring between enzyme monomers and dimers. The different UV−vis spectrum observed for this species, as compared to the enzyme resulting from slow addition of metal, suggests that this exchange is associated with a chemical modification of the enzyme. The new conformation is different from that formed during the pH titration of CuDAHPS under basic conditions but may be related to the copper−enzyme complex that is observed following the addition of Cu^{2+} to apoDAHPS that has been cycled to pH = 10.

Analysis of the EPR spectra shows two different conformations at pH = 7.0 for both Cu^{2+}- and Mn^{2+}-substituted complexes. For CuDAHPS there is a significant difference between these two species. It is possible to predict the charge and ligand set for copper complexes using a Peisach−Blumberg plot of $g_{||}$ versus $A_{||}$ (*43*). The relative positions for the $g_{||}$ and $A_{||}$ values determined from this work on such a plot are shown as crosses in the Supporting Information (Figure S1). Both species observed at pH = 7 fall slightly below the predicted region for mixed nitrogen and oxygen coordination. This is generally assumed to be due to a deviation from axial symmetry. In general, sulfur coordination to copper usually leads to a smaller value for $g_{||}$ than nitrogen coordination. There are few examples of Cu^{2+} coordination to a single sulfur ligand in type 2 (nonblue) copper complexes. On the basis of the behavior of the system in basic conditions we believe that sulfur is not a metal ligand at pH = 7.0. The two new points marked on the Peisach−Blumberg plot in the Supporting Information (Figure S1) form a line that is approximately parallel to the boundary line. The difference between them, therefore, suggests that there is a change in the ligand set or charge of the complex. The first species lies toward the bottom of the range for a dinitrogen/dioxygen donor atom coordination. The second species lies in an area where dinitrogen/dioxygen and tetranitrogen donor atom sets all overlap. Within the same coordination set there is a progression of decreasing $g_{||}$ and increasing $A_{||}$ with decreasing charge on the complex. The signal intensities for the two species are roughly equal, suggesting that they are present in approximately equal amounts. Possibilities for the groups and transformations are deprotonation of His268, Cys61, or a coordinated water molecule, but the limited pH stability range for this protein prevents making a more comprehensive examination of the pH-dependent spectroscopic changes impossible. If the ligand set were to change, it would probably be from dinitrogen/dioxygen to trinitrogen/oxygen. In the crystal structure of PbDAHPS(Phe), only a single nitrogen ligand was bound to the Pb^{2+}, with the same being true for the MnDAHPS-(Phe) structure. This fact, along with the behavior on titration with base, suggests that this change is less likely. Another possibility for the different species relates to the aggregated state of the enzyme.

In the crystal structure of MnDAHPS the long Mn−S separation, 2.74 Å, was interpreted as a bonding interaction (*21*). The rmsds for the bond lengths in this determination are listed as 0.012 Å, and given that this particular separation is for the only two vicinal non first row elements in this structure, this must be considered the upper limit for the Mn−S separation. Thus a liberal estimate of the Mn−S separation range is 2.62−2.86 Å. We note that the corresponding range for Mn(II)−SR bond lengths from high-resolution small molecule X-ray crystal structures is 2.393−2.429 Å, for nonchelating thiolate donors to Mn(II) (*44*). Thus any Mn−S interaction can only be described as either nonexistent or, at the very most, weak, if present at all. The spectroscopic results in this paper clearly indicate that in CuDAHPS this interaction is absent.

We suggest that, at pH 7.0, the Cu^{2+} coordination sphere is either a dinitrogen/dioxygen or a mononitrogen/trioxygen ligand set in a distorted axial environment. His268 is certainly one of the nitrogen ligands. In the first possibility, the second nitrogen donor atom could possibly come from Lys97, the next closest nitrogen ligand. In the crystal structure of DAHPS(Phe) (*20*) Lys97 hydrogen bonds to a water molecule coordinated to Pb^{2+} and to PEP. If the water molecule was displaced, this may allow rearrangement of Lys97 to become a ligand. In either possibility, two of the oxygen donors could come from Glu302 and Asp326, both of which are within 3 Å of the Pb^{2+} center, or a combination of one of these ligands and a coordinated water molecule. This situation is also true for the MnDAHPS(Phe) structure. We favor one acidic residue and a coordinated water molecule, which can be deprotonated to the hydroxide, but are unsure of how this would correlate with the geometry of the binding site. It was recognized by Bauerle et al. that the Pb^{2+} ion occupies a much larger volume than other divalent metal ions, which activate the enzyme, while lead does not, and hence different coordination patterns may be observed at the metal binding site (*20*). This is not uncommon. The iron transport protein transferrin is capable of binding a variety of different metal ions in vitro, all with different association constants. Spectroscopic and crystallographic studies have shown that the coordinating ligand set can vary depending upon the metal bound (*45*, *46*). However, the recent structure of the MnDAHPS(Phe) suggests that, at least at pH = 8.7, the coordinating ligands do not change when Pb^{2+} is substituted with Mn^{2+} (*21*).

The observations from the UV−vis and EPR spectra for titration of CuDAHPS(Tyr) with base indicate that there is a conformational change between pH = 7.0 and pH = 8.7. The isobestic behavior of the UV−vis spectrum suggests a simple transition between two species, such as a change in charge or ligand set of the complex. The EPR spectra are not as clear-cut with significant changes in $g_{||}$ and $A_{||}$. At the intermediate region pH = 7.5 two species can be identified: a minor component, which is also observed at pH = 7.0, and a major component, which appears closely related to the final product at pH = 8.7. It is likely that these two

species contain the same ligand set but have different outer shells. This is supported by the fact that addition of PEP to the sample at pH = 8.7 alters the EPR spectrum so that it closely relates to that measured at pH = 7.0 in the absence of PEP. When the $g_{||}$ and $A_{||}$ values, for the species at pH = 8.7, are added to the Peisach−Blumberg plot in Figure S1, they fall in a region different from that observed for the two complexes at pH = 7.0. This is within the normal regions predicted and suggests a slight change in geometry to a more closely axial system. In this region of Figure S1 mononitrogen/tetraoxygen, dinitrogen/dioxygen, trinitrogen/oxygen, and tetranitrogen donor atom sets are expected to overlap.

The small changes observed in the EPR spectrum, following the addition of the substrate PEP, indicate that it is not a direct ligand but does have an effect on the metal center. The main differences are based upon a change in the hyperfine coupling of the $g_{\perp}$ region, which is based upon interactions with surrounding nitrogen ligands and possibly the copper nucleus itself. It is interesting, therefore, to note that from the crystal structure His268 serves as a ligand to both PEP and Pb^{2+}. As a result of this, the residue is in a strained conformation, and this could be the basis for the changes in the EPR spectrum. Recent work has focused some attention on the metal center of DAHPS. It is expected that further work by ourselves, and others, based upon spectroscopic studies and X-ray crystallography of DAHPS containing different metals, will sharpen this picture and help to determine the role of the metal in the enzymatic mechanism.

CONCLUSIONS

Previously it has been shown that DAHPS(Tyr), in common with other members of this enzyme family, can bind a variety of different metal ions to generate an active enzyme complex (*7*, *11*, *13*, *15*). The data presented here demonstrate that there are a number of different enzyme conformations, which can be characterized by their different spectroscopic signatures. These conformations are likely to differ in terms of the charge and ligand set of the metal center. The conformation adopted is affected by a number of factors, including the pH and the manner of metal addition, and is an important consideration in sample preparation. The addition of the substrate PEP leads to only minor alterations in the EPR spectrum of CuDAHPS(Tyr). This is consistent with the sharing of a common enzyme residue (His268) but no direct metal−substrate interaction.

SUPPORTING INFORMATION AVAILABLE

Figure S1 showing a Peisach−Blumberg plot for the two conformers of CuDAHPS. This material is available free of charge via the Internet at http://pubs.acs.org.

REFERENCES

1. Cohn, E. E. (1985) *The Shikimic Acid Pathway*, Vol. 20, Plenum Press, New York.
2. Srinivasan, P. R., and Sprinson, D. (1959) *J. Biol. Chem. 234*, 716−722.
3. Bonner, C. A., Fischer, R. S., Schmidt, R. R., Miller, P. W., and Jensen, R. A. (1995) *Plant Cell Physiol. 36*, 1013−1022.
4. Walker, G. E., Dunbar, B., Hunter, I. S., Nimmo, H. G., and Coggins, J. R. (1996) *Microbiology 142*, 1973−1982.
5. Doy, C. H., and Brown, K. D. (1965) *Biochim. Biophys. Acta 104*, 377−389.
6. Baasov, T., and Knowles, J. R. (1989) *J. Bacteriol. 171*, 6155−6160.
7. Davies, W. D., and Davidson, B. E. (1982) *Nucleic Acids Res. 10*, 4045−4048.
8. Ray, J. M., Yanofsky, C., and Bauerle, R. (1988) *J. Bacteriol. 170*, 5500−5506.
9. Shultz, J., Hermodson, M. A., Garner, C. C., and Herrmann, K. M. (1984) *J. Biol. Chem. 259*, 9655−9661.
10. Stephens, C. M., and Bauerle, R. (1991) *J. Biol. Chem. 266*, 20810−20817.
11. Ramilo, C. A., and Evans, J. N. S. (1997) *Protein Expression Purif. 9*, 253−261.
12. DeLeo, A. B., Dayan, J., and Sprinson, D. B. (1973) *J. Biol. Chem. 248*, 2344−2353.
13. Dusha, I., and Denes, G. (1976) *Biochim. Biophys. Acta 438*, 563−573.
14. McCandliss, R. J., and Herrmann, K. M. (1978) *Proc. Natl. Acad. Sci. U.S.A. 75*, 4810−4813.
15. Nagano, H., and Zalkin, H. (1970) *Arch. Biochem. Biophys. 138*, 58−65.
16. Schoner, R., and Herrmann, K. (1976) *J. Biol. Chem. 251*, 5440−5447.
17. Sundaram, A. K., Howe, D. L., Sheflyan, G. Y., and Woodard, R. W. (1998) *FEBS Lett. 441*, 195−199.
18. Weaver, L. M., Pinto, J. E. B. P., and Herrmann, K. M. (1993) *Bioorg. Med. Chem. Lett. 3*, 1421−1428.
19. Doong, R. L., Ganson, R. J., and Jensen, R. A. (1993) *Plant, Cell Environ. 16*, 393−402.
20. Shumilin, I. A., Kretsinger, R. H., and Bauerle, R. (1999) *Structure 7*, 865−875.
21. Wagner, T., Shumilin, I. A., Bauerle, R., and Kretsinger, R. H. (2000) *J. Mol. Biol. 301*, 389−399.
22. Akowski, J. P., and Bauerle, R. (1997) *Biochemistry 36*, 15817−15822.
23. Stephens, C. M., and Bauerle, R. (1992) *J. Biol. Chem. 267*, 5762−5767.
24. Kikuchi, Y., Tsujimoto, K., and Kurahashi, O. (1997) *Appl. Environ. Microbiol. 63*, 761−762.
25. Ger, Y.-M., Chen, S.-L., Chiang, H.-J., and Shiuan, D. (1994) *J. Biochem. 116*, 986−990.
26. Park, O. K., and Bauerle, R. (1999) *J. Bacteriol. 181*, 1636−1642.
27. Doong, R. L., and Jensen, R. A. (1992) *New Phytol. 121*, 165−171.
28. Bradford, M. M. (1976) *Anal. Biochem. 72*, 248−254.
29. Holm, R. H., Kennepohl, P., and Solomon, E. I. (1996) *Chem. Rev. 96*, 2239−2314.
30. Froncisz, W., and Aisen, P. (1982) *Biochim. Biophys. Acta 700*, 55−58.
31. Bonomo, R. P., and Riggi, F. (1982) *Chem. Phys. Lett. 93−96*, 90.
32. Pandeya, K. B., and Patel, R. N. (1992) *Indian J. Biochem. Biophys. 29*, 242−250.
33. Rakhit, G., Antholine, W. E., Froncisz, W., Hyde, J. S., Pilbrow, J. R., Sinclair, G. R., and Sarkar, B. (1985) *J. Inorg. Biochem. 25*, 217−224.
34. Ovchinnikov, I. V., and Konstantinov, V. N. (1978) *J. Magn. Reson. 32*, 179−190.
35. Lee, S. (1981) *Phys. Rev. B 23*, 6151−6153.
36. Hyde, J. S., and Froncisz, W. (1982) *Annu. Rev. Biophys. Bioeng. 11*, 391−417.
37. Pilbrow, J. R. (1990) *Transition Ion Electron Paramagnetic Resonance*, 1st ed., Clarendon Press, Oxford.
38. Banci, L., Bencini, A., Benelli, C., Gateschi, D., and Zanchini, C. (1982) *Struct. Bonding 52*, 37.
39. Coffino, A. R., and Peisach, J. (1996) *J. Magn. Reson. B 111*, 127−134.
40. Aasa, R., and Aisen, P. (1968) *J. Biol. Chem. 243*, 2399−2404.
41. Sheflyan, G. Y., Howe, D. L., Wilson, T. W., and Woodard, R. W. (1998) *J. Am. Chem. Soc. 120*, 11−27−11032.

42. Subramaniam, P. S., Xie, G., Xia, T., and Jensen, R. A. (1998) *J. Bacteriol. 180*, 119−127.
43. Peisach, J., and Blumberg, W. E. (1974) *Arch. Biochem. Biophys. 165*, 691−708.
44. *Cambridge Crystallographic Data Base, Version 2.37*, Vol. 1998, Cambridge Crystallographic Data Centre, Cambridge, England.
45. Smith, C. A., Anderson, B. F., Baker, H. M., and Baker, E. N. (1992) *Biochemistry 31*, 4527−4533.
46. He, Q.-Y., Mason, A. B., Woodworth, R. C., Tam, B. M., MacGillivray, R. T. A., Grady, J. K., and Chasteen, N. D. (1997) *Biochemistry 36*, 14853−14860.
47. Matzanke, B. F., Müller-Matzanke, G., and Raymond, K. N. (1989) *Iron Carriers and Iron Proteins* (Loehr, T. M., Ed.) pp 1−122, VCH, Weinheim.

BI010238F